

# International Journal of Nanoelectronics and Materials

MeaNCI

ISSN 1985-5761 | E-ISSN 2232-1535



## Radiation's impact on PANI nanoparticles' optical and dielectric properties

Shawkat Salameh Gasaymeh a\*; Aeshah Salem b

- <sup>a</sup> Department of General Education Abu Dhabi Polytechnic Al Ain, United Arab Emirate
- <sup>b</sup> Department of Physics Faculty of Science Taibah University Yanbu 46423, Saudi Arabia
- \*Corresponding author. Tel.: +971501731969; e-mail: shawkat.gasaymeh@actvet.gov.ae

Received 26 October 2024, Revised 28 February 2025, Accepted 16 April 2025

#### **ABSTRACT**

Additional information is provided regarding the precise doping processes used on PANI nanoparticle samples. This method involves polymerizing aniline monomer into conductive PANI emeraldine salt (ES) using dodecylbenzenesulfonic acid (DBSA) as an accelerator and dopant, in addition to the oxidizing agent and ionizing  $\gamma$ -irradiation. This fast one-step technique produces PANI straight from its monomer. The interactions in this synthesis technique stimulate the development of longer PANI chains, which improves solubility, thermal stability, and conductivity. Adding DBSA, a long-chain organic acid, as a dopant ion during  $\gamma$ -irradiation improves the optical and dielectric properties of the PANI nanoparticles. Thermogravimetric analysis (TGA) data confirms that the thermal stability of the PANI nanoparticles increases with larger doses of gamma radiation. In the range above 370 to 600°C indicating some structural decomposition of the polymer backbone. This may be due to acid hydrolysis causing chain scission during the polymerization process under the impact of  $\gamma$ -irradiation. The direct double-doping approach using  $\gamma$ -rays and DBSA in a single step eliminates the requirement for the typical synthesis process for these nanomaterials with long-chain dopant ions, therefore avoiding time-consuming stages like de-doping and re-doping.

Keywords: Nanoparticles, PANI, nanocomposite, dopant, optical and dielectric properties and irradiation

### 1. INTRODUCTION

Recent years have seen an increase in scientific and technological interest in polymer systems with unique properties. These systems provide an enormous array of potential new materials that can be created and have a wide range of electrical, optical, and magnetic capabilities. The repeatable management of the macromolecular's supramolecular and molecular architecture through an easy-to-follow organic synthesis process is essential for technological applications. Polyaniline (PANI) is a conductive polymer that can be manufactured with no special equipment or precautions. Because conducting polymers usually exhibit highly reversible redox activity with detectable chemical memory, they have been regarded as major innovative materials for the creation of devices such as industrial sensors. [1-4]. Doping amount, protonation level, dopant ion size, and water content all have a substantial influence on the characteristics of conducting polymers. Conducting PANI is produced by either chemical oxidative polymerization electrochemical oxidative polymerization [1,4-7]. The electrical insulator known as the emeraldine base (EB) type of PANI is composed of two nitrogen atoms from an amine and two nitrogen atoms from an imine. Protonic acid doping and oxidative doping are two different doping strategies for converting PANI EB into a conducting state [7-10]. The process of protonating imine nitrogen atoms without exchanging electrons is known as protonic acid doping of emeraldine bases. Leucoemeraldine undergoes oxidative doping to form ES through electron exchange.

The presence of the -NH group in the polymer backbone is thought to be the primary source of structural modifications, as protonation and deprotonation affect the polymer's electrical conductivity and color [1,10, 11].

When organic and inorganic acids are employed to protonate the emeraldine base, the ES PANI is formed. This practice is usually known as doping. When PANI, in the form of an emeraldine base, is treated with acids, protons interact preferentially with nitrogen imine atoms, leading to the production of polycations [9-12]. As a result, the acids HCl and H<sub>2</sub>SO<sub>4</sub> are regarded to be the most effective dopants for protonating PANI. The lone electron pair of nitrogen atoms "unpairs" without changing the system's electron count because electron density tends to redistribute due to positive charges focused on neighboring nitrogen atoms, which raises the total energy of the polymer system [12-15]. When polymers are subjected to γ-radiation, they scission and liberate molecules, atoms, and fragments of molecules, causing structural defects and the original structure to break down [16-18]. Scission, cross-linking, or both may be induced, and a variety of charged species, ions, and free radicals are generated. This results in changes to the molecular weight, solubility, and optical and characteristics, and it is dependent on the energy of the ionization radiation and the polymer's composition. However, the radiation method has proven to be a costeffective and environmentally friendly approach for producing large quantities of metal nanoparticles with tunable sizes and structures [1,15]. Furthermore, the obtained results demonstrate superior performance compared to those achieved through alternative methods.

#### 2. EXPERIMENTAL PROCEDURE

A hybrid chemical technique was used to oxidize an aniline monomer by  $\gamma$ -irradiation, resulting in PANI ES, the conductive form. If DBSA is present, radiation may alter the polymer. Additionally, reactions between gases or polyaniline molecules and  $\gamma$ -ray photons can indirectly produce ionic species. Secondary electron collisions, rather than direct  $\gamma$ -ray excitation, lead to ionization. Furthermore, exposure to radiation drops the polymer and may not affect its oxidation state. We previously released the materials, PANI nanoparticle formation under gamma radiation, together with the procedures for setup. For additional details, refer to [1].

## 3. PANI NANOPARTICLES' UV-VIS SPECTRA

Figure 1 illustrates the UV-VIS spectra of the irradiationgreen-filtered PANI nanoparticle suspension acquired during our investigation, which shows three principal absorption peaks. The first peak, which appears at around 800 nm, is caused by electrical changes in the C=N bond, or electron migration from the benzenoid to the quinoid rings. This could be because the imine group, which symbolizes the polarons and produces the color green, creates a C=N double bond when PANI is used. The third absorption peak at 350 nm, which is linked to the  $\pi$ - $\pi^*$  transition of the benzenoid ring, and the second peak at 423 nm, which represents the  $\pi^* \leftarrow \pi$  transition in polaron/bipolaron and is connected to the polaron band transitions, both suggest the presence of the polymer in its ES state, the conductive form of PANI [1,2,19]. A conductive ES spectrum of PANI that typically is comprised of these three peaks. This ES spectra is comparable to that of bulk PANI produced in the solution phase under chemical experimental conditions [20].

The production of conductive polyaniline is characterized by the longitudinal peak at 800 nm. Molecular orbitals serve as the foundation for UV-Vis spectroscopy's operation. Bonding and anti-bonding orbitals, which are created by adding or deleting the appropriate atomic orbitals, are the molecular orbitals found in all compounds. A molecule's valence electrons are located in the bonding orbital, also known as the highest occupied molecular orbital (HOMO). In contrast, the anti-bonding orbital, also known as the lowest unoccupied molecular orbital (LUMO), is usually electron-free. This is an ideal description that only applies to individual molecules. Actually, a bulk material is composed of several atoms assembled together. In this case, the LUMOs and HOMOs of each atom are combined to form a large number of closely spaced orbitals, or bands. The two distinct bands that form are known as the conduction band (CB) and valence band (VB). Conduction band electrons are more widely separated from their particular nuclei, allowing for free movement

within the material, while VB electrons are securely bonded to their unique nuclei

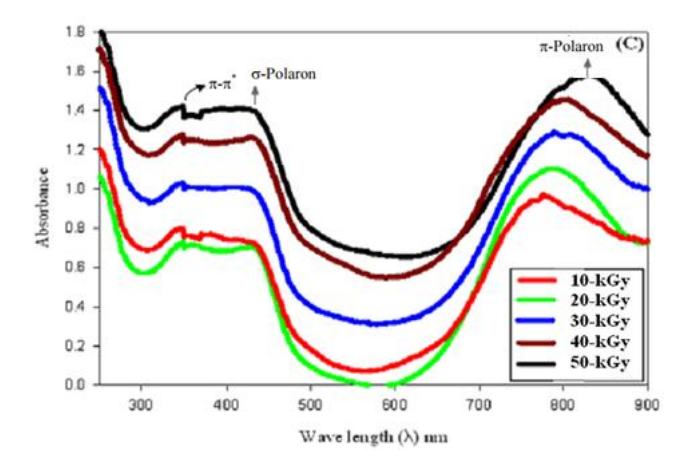


**Figure 1**. Absorption UV-vis spectra of PANI nanoparticles produced at different dosages

The UV-visible absorption spectra results support the previously published suggested production technique [1]. However, low-dose  $\gamma$ -irradiation of the PVP ES PANI is expected to produce more C-OH and C-H side chain scissions because C-C bonds have a much higher binding energy than C-OH and C-H bonds [1-4]. Novel bonds like C=O and C=C will form in aldehyde molecules as a result of increased C-OH covalent bond scissions brought on by higher dosages [1,21]. According to UV-vis analyses, the C=N double bonds that develop in the imine groups as the dosage rises are what give PANI its green color and increased intensity.

## 3.1 The Optical Band Gap Energy

The optical band gap energy in a semiconductor is found by graphing the absorption coefficient  $\alpha(v)$   $\alpha(v)$  as  $\alpha(v)hv)1/m$  vs. hv, where m indicates the kind of transition and hv is the photon energy [1,4,20,21]. For permissible, approved indirect, forbidden, and prohibited direct transitions, their values can be ½, 2, 3/2, or 3, respectively. Nevertheless, the PANI nanoparticles' band gap analysis showed that when the band gap energy dropped, the gamma dosage and/or DBSA concentration increased.

Free acid, dilution, interference from the oxidant's ionic byproducts, and the fact that more electrons are created as the gamma dose rises, which suggests the production of a more conductive ES with a high protonation level, all contribute to the observed behavior. In essence, photons from UV-visible light sources with energies higher than the band gap energy will be absorbed by the materials under study. Electronic transitions from the HOMO  $\pi$ -band to the LUMO  $\pi^*$ -band are associated with absorption [21–24]. The absorption edge, the lowest energy level in the band gap between the VB's HOMO and the CB's LUMO, is where electronic transitions between the valence and conduction bands start.

Graphs of  $(\alpha(v)hv)^2$  vs. hv for PANI nanoparticles distributed in PVP at different DBSA concentrations have

been previously presented and discussed in [1]. In order to determine the direct band gap energy of PANI nanoparticles in PVP, Mott and Davis [25] recommend utilizing the curves at  $(\alpha(v)hv)^2 = 0$ . However, the results show that the band gap Eg value decreases as the gamma radiation increases.

The optical band gap energy decreases with increasing radiation dosage. For the  $\pi\text{-}\pi^*$  electronic transition, the irradiation composite produces more polarons, which decreases the band gap between the valence band (VB) and conduction band (CB), thereby increasing conductivity. The observed decrease in the band gap energy gap of the increased irradiation, which is consistent with the formation mechanism proposed in previous studies [1], lends support to this. The energy band gap was reported to decrease from 1.32 eV to 1.0 eV as the dose increased from 10 kGy to 50 kGy [1,25]. Additionally, the irradiation composite's increased polaron concentration results in a smaller band gap for the  $\pi\text{-}\pi^*$  electronic transition.

Additionally, polymers can be doped with radiation. A summary provided by [1-4,26,27] stated that radiation can alter polymers chemically by causing chain scission, crosslinking, C=C creation, alkyne group production, and reduction of heteroatoms, such as sulfur, nitrogen, or oxygen. Furthermore, the same outcome was noted in a lengthy investigation conducted in polycarbonate using irradiation-induced years ago by references therein [28,29].

The primary effects of radiation on polymers include chain scission and other alterations that improve their optical properties. Therefore, the band gap energy was reduced by utilizing two doping strategies: DBSA acid and gamma irradiation. This was due to the radiation-induced sharp increase in intercluster interactions. Following the application of DBSA and  $\gamma$ -irradiation, they made the unexpected discovery that, as suggested by the proposed creation mechanism, higher dopant levels result in higher protonation levels with more polarons. This is because the same degree of doping is employed for both the DBSA and gamma inter-chain interactions. Our UV-vis study of DBSA also showed a red shift because the drug reduces the pH of the medium; this leads to a decrease in the band gap due to greater protonation.

## 4. THE DIELECTRIC PROPERTIES OF PANI NANOPARTICLES

The dielectric constant (E') and dielectric loss (E'') for PANI nanoparticles synthesized at various  $\gamma$ -irradiation dosages ranging from 10 to 50 kGy in steps of 10 kGy are plotted against log frequency in Figures 2 and 3, respectively. For all irradiated PANI samples, a significant drop in the dielectric loss and dielectric constant has been noted with increasing frequency. A steady approach to the charge carriers' resonance frequency along the polymeric chains is shown by the significant decline in both the dielectric constant and the dielectric loss at higher frequencies [29-

31]. The tendency of dipoles in macromolecules to align themselves with the applied field at low frequencies may be the cause of the sharp decline in dielectric constant with increasing frequency. Singh and Gupta also noted this phenomenon in their investigation of dielectric relaxation in polymer (PVA-H<sub>3</sub>PO<sub>4</sub>) electrolytes. Higher frequencies result in a change in the direction of polarization, which lowers the dielectric constant and dielectric loss. The charge carriers go across the dielectric, become trapped against the faulty sites, and create an opposing charge nearby. The dielectric constant, however, falls in the highfrequency range because the dipoles would find it difficult to align themselves with the applied field [32,33]. Furthermore, when the γ-influence increases, so do the PANI nanoparticles' dielectric constant and dielectric loss. The creation of conjugated double bonds as a result of yirradiation, or the formation of the conductive form of PANI ES at higher doses, is responsible for this rise in both the dielectric constant and the dielectric loss. For several polymers exposed to ion beams, the same outcome has been noted: irradiation causes  $\pi$ -electron clouds to develop, with the polarization oriented in the direction of the molecular chains [1-4].

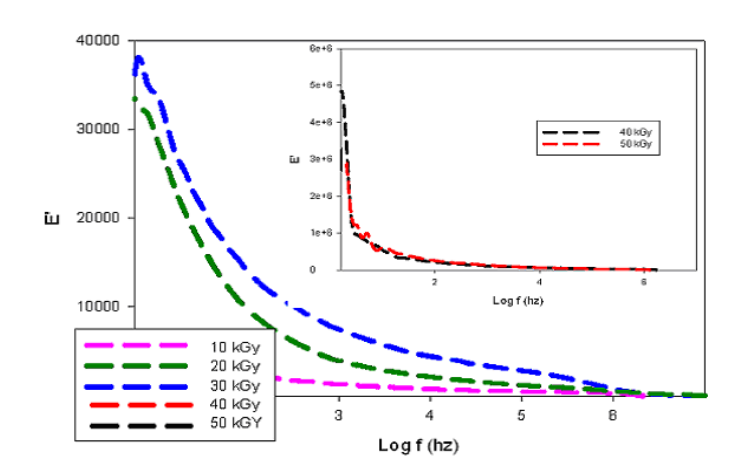


**Figure 2**. Dielectric constant of PANI nanoparticles produced at various gamma irradiation levels as a function of log frequency

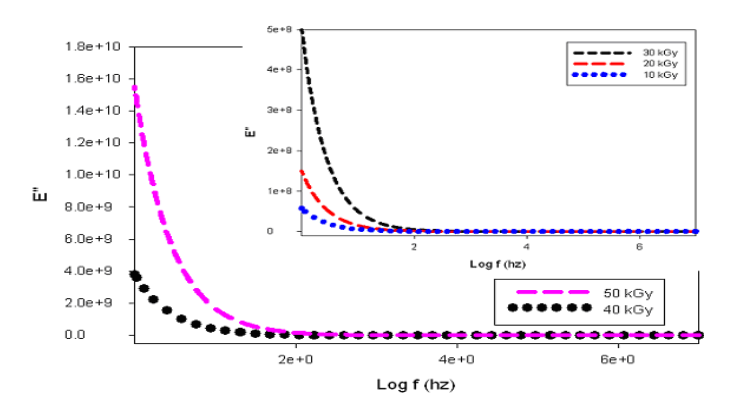


**Figure 3**. Dielectric loss of PANI nanoparticles produced at various gamma irradiations as a function of log frequency

The low amount of protonation of the PANI chains, which results in fewer polarons being generated, may be the cause of the reduced dielectric constant and dielectric loss of PANI nanoparticles at low irradiation doses. The enhancement of PANI nanoparticles' dielectric constant and dielectric loss results from the beneficial effects of  $\gamma$ -rays on the salt form of PANI synthesis, as demonstrated by UV studies, and their smaller size and improved distribution, as observed in SEM, which promotes better electronic transport.

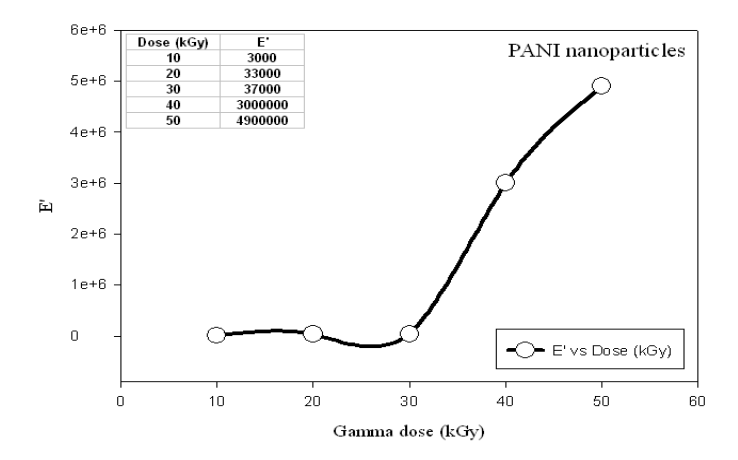


**Figure 4**. Dielectric constant vs. gamma irradiation dose for PANI nanoparticles

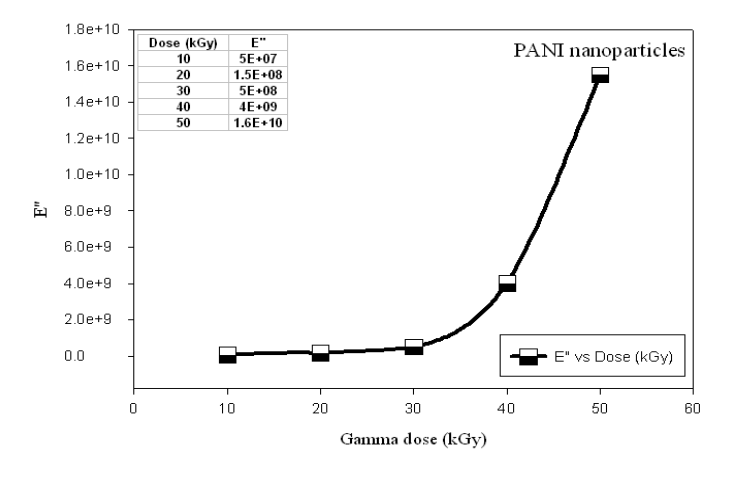


**Figure 5**. Dielectric losses vs. gamma irradiation dose for PANI nanoparticles

Under the influence of gamma irradiation, the dielectric constant increases from 3 x 10<sup>3</sup> at 10-kGy to 33 x 10<sup>3</sup> at 20 kGy, then increases to  $37 \times 10^3$  at 30-kGy and then to  $3 \times 10^3$ 106 at 40-kGy and reach the maximum to be 49 x 105 at 50kGy as presented in Figure 4. On the other hand, the dielectric loss increases from 5 x 10<sup>7</sup> at 10-kGy to 15 x 10<sup>7</sup> at 20-kGy to 5 x 108 at 30-kGy to 4 x 109 at 40-kGy and then to be 1.6 x 10<sup>10</sup> at 50-kGy as shown in Figure 5. In addition to the creation of conductive islands (double-bonded carbonaceous clusters), scissioning of the polymer chain may be the cause of the rise in dielectric constant and dielectric loss brought on by intense γ-irradiation. Gasaymeh reported similar outcomes in the case of protonirradiated polymers, which were ascribed to increased protonation and the formation of more polaron as a result of a higher irradiation dosage [1-4]. The noticeable increase in both the dielectric constant (E') and dielectric loss (E") at doses above 30 kGy can be attributed to the

enhanced formation of polarons and bipolarons within the PANI matrix under higher  $\gamma$ -irradiation doses. These charge carriers increase the interfacial polarization and conductivity of the nanocomposite, especially at low frequencies. Moreover, the higher radiation dose may induce more structural defects and promote chain scission, resulting in increased mobility of charge carriers and dipolar alignment, which contributes to the observed enhancement in dielectric properties at 40 and 50 kGy

### 5. THERMAL GRAVIMETRIC ANALYSIS (TGA)

Some of the generated samples were subjected to TGA measurements. A known weight of the composites was heated from room temperature to  $600\,^{\circ}$ C, which is between the solvent's boiling point and the polymer's breakdown temperature, at a rate of  $10\,^{\circ}$ C/min.

Figure 6 displays the weight loss of PANI nanoparticles at varying irradiation doses as a function of temperature. Chain scission, cross-linking, and changes in the chemical composition, structure, and constitution of polymers are caused by ionizing radiation. These changes include the production of C=C, the formation of alkyne groups, and the depletion of heteroatoms, such as N, S, or O [1-4,34-37]. Compared to the traditional oxidation polymerization method via chemical and electrochemical means, this might improve thermal stability [37-39]. However, the findings indicated that the molecular weight and crystallinity at the primary decomposition temperature can influence the thermal stability of PANI nanoparticles. This tendency is consistent with modest structural change. Consequently, weight loss diminishes as γ-dose rises. The outcome shows that γ-irradiation causes nanoparticles with a reduced molecular weight to develop.

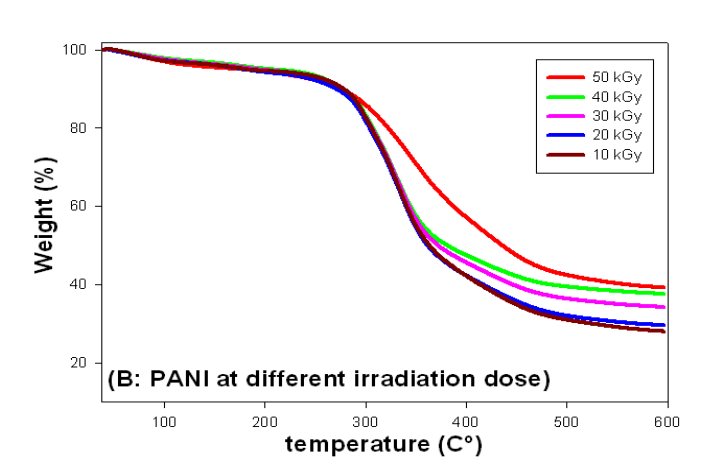
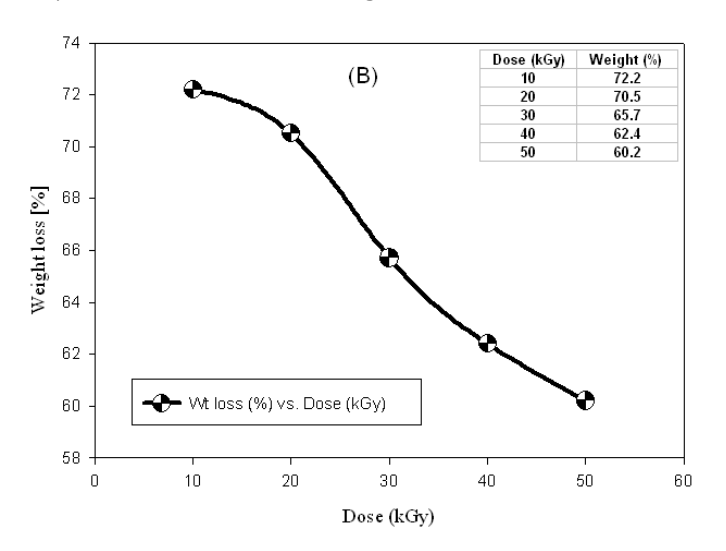


Figure 6. displays the PANI/DBSA nanoparticles' TGA thermogram made at various γ-doses

The decomposition temperatures obtained from TGA thermogram of PANI nanoparticles exhibit two-step weight loss behavior. The first loss of weight appears below 140°C and is contributed by the elimination of impurities, residual water, and unreacted monomers. The evaporation and

degradation of DBSA is represented by the second weight loss that begins at about 250 °C. At this point, the polymer chain and the dopant (DBSA) no longer interact through the NH+...SO3– interaction, and DBSA breakdown begins. Pure DBSA starts to degrade at about 250 °C [38]. As a result, the doped PANI nanoparticles' initial degradation temperature is greater than that of the pure DBSA and shifts to a higher temperature range as the system's gamma dosage increases.

Moreover, there is a noticeable weight loss stage, starting at above 370 °C up to around 500 °C, is assigned to structural decomposition of the polymer backbone. The more thermal stability as  $\gamma$ -doses increase could be attributed to the better order structure in the nanoparticle, as the influence of irradiation may hinder the heat accumulation between the particles. The weight loss of the thermal decomposition versus  $\gamma$ -doses (kGy) of the synthesized PANI nanoparticles is illustrated in Figure 7. The TGA analysis presented in Figure 7 covers a temperature range from room temperature up to approximately 600 °C, clearly demonstrating the influence of  $\gamma$ -irradiation on thermal degradation behavior



**Figure 7**. Weight loss of PANI nanoparticles produced at varying radiation intensities as measured by TGA thermogram

As any of the aforementioned parameters (dose and DBSA dopants) increased, PANI nanoparticles showed a greater degradation temperature, indicating a decrease in weight loss. This may be due to acid hydrolysis causing the sample's chain scission during the polymerization process under  $\gamma$ -irradiation's effect. Moreover, the presence of DBSA when exposed to  $\gamma$ -irradiation may cause morphological changes within the polymer and is shown by the SEM micrographs [1-4].

In this study, the  $\gamma$ -irradiation method resulted in superior performance of PANI nanoparticles compared to conventional synthesis techniques. Specifically, the conductivity of  $\gamma$ -irradiated PANI was 20% higher than that obtained using chemical oxidative polymerization methods

(40). Similarly, the dielectric constant of  $\gamma$ -irradiated PANI showed a 15% increase, surpassing the values reported by conventional electrochemical methods (41). Furthermore, the thermal stability of the  $\gamma$ -irradiated PANI nanoparticles was enhanced by 10% compared to those synthesized by traditional methods, as demonstrated by the TGA analysis (42). These improvements highlight the effectiveness of  $\gamma$ -irradiation in enhancing key properties of PANI nanoparticles, making it a promising technique for the synthesis of high-performance conducting polymers.

#### 6. CONCLUSIONS

The objective of this article is to create a novel technique for manufacturing conducting nanomaterials using γ-ray radiation. The potential of γ-irradiation strategies to enhance the optical and dielectric characteristics of manufactured nanocomposites in the presence of protonated DBSA has been investigated. As a result of the loss of  $SO_3^-$ , DBSA experiences high-degree side chain degradation during y-irradiation. The aniline monomer is subsequently "in situ", polymerized into ES state the conducting form PANI, by using this oxidant effect to dope the aniline imine group. When studying the optical characteristics of PANI nanoparticles, UV-Vis spectroscopy was utilized. This method confirmed the synthesis of PANI by showing that the absorption level at the 800 nm band for conducting PANI showed an exponential increase with higher dosage (kGy) and/or the addition of DBSA. Visual examination of the composites revealed that they changed color from colorless to dark green. When compared to PANI nanoparticles made by chemical and electrochemical processes, our PANI nanoparticles exhibit a superior protonation of the PANI backbone due to their greater wavelength, which occurs around the peak of 800 nm. The usage of DBSA doping under radiation impacts the charge carriers. One way that doping affects PANI is by increasing the mobility of charge carriers and the density, which raises the ratio of bipolaron to polaron and forms a conductive form.

These findings demonstrate that the conductivity, dielectric constant, dielectric loss, and optical band gap all reach optimal values at a dopant concentration and dose, which meets our goal. Furthermore, these evenly distributed nanoparticles of PANI functioned as mini capacitors in the composites. Therefore, the buildup of these nano-sized capacitors is responsible for the PANI composite material's high dielectric constant. The charge linked with a single particle was limited to that particle since these nanoparticles were lodged within the PVP; for larger particles, the charge could not move to nearby particles. On the other hand, as dosage, DBSA, and aniline rose in the system because of the development of the conductive form of PANI (ES), more charge carriers could be produced, expanding the dielectric characteristics on the protonation level. As a result, the chain broke up into smaller pieces, and the dielectric properties increased with the addition of aniline monomer, DBSA, and gamma radiation. Exposure to radiation produces this effect.

Changes in material characteristics, including an increase in dielectric constant and loss, can result from scissioning under high  $\gamma$ -irradiation. This results from modifications to the material's molecular structure, which affect how the material responds to electric fields.

The research of conducting polymers has several opportunities. It is now possible to design and construct conducting PANI-based devices even if the charge transfer properties of conducting polymers are still unclear. This is due to the reproducibility of electrical, optical, and other features. It is suggested that this study's next phase focus on developing gadgets that would be superior to those constructed of traditional materials in a number of ways. Furthermore, the semiconductor industry, photovoltaic cells, sensor materials, and photonic band gap materials all of which have not yet been fully explored can employ nanostructured polymers. Moreover, multiple additional conducting polymers should be involved in the  $\gamma$ -ray radiation polymerization process.

#### REFERENCES

- [1] S. S. Gasaymeh, "Formation mechanism and characterization of PANI nanoparticles by hybrid chemical and gamma irradiation technique," \*American Journal of Applied Sciences, vol. 15, no. 12, pp. 519-531, 2018, doi: 10.3844/ajassp.2018.519.531.
- [2] S. S. Gasaymeh, S. Radiman, L. Y. Heng, E. Saion, and G. H. M. Saeed, "Synthesis and Characterization of Silver/Polyvinylpyrrolidone Nanoparticles Using Gamma Irradiation Techniques," \*African Physical Review\*, vol. 4, 2010, p. 0006.
- [3] S. S. Gasaymeh, S. Radiman, L. Y. Heng, and E. Saion, "Gamma Irradiation Synthesis and Influence the Optical and Thermal Properties of Cadmium Sulfide (CdS)/Poly (Vinyl Pyrolidone) Nanocomposites," \*American Journal of Applied Sciences\*, vol. 7, no. 4, pp. 500-508, 2010.
- [4] S. S. Gasaymeh and N. N. Almansoori, "Novel formation mechanism of Ag/PANI/PVP core-shell nanocomposites," \*Results in Physics\*, vol. 16, 2020, doi: 10.1016/j.rinp.2019.102882.
- [5] A. A. Ahmad et al., "Synthesis and Characterization of ZnO NPs-Doped PMMA-BDK-MR Polymer-Coated Thin Films with UV Curing for Optical Data Storage Applications," \*Polymer Bulletin\*, vol. 78, pp. 1189-1211, 2021, doi: 10.1007/s00289-020-03155-x.
- [6] E. E. V. Chapman, C. Moore, and L. M. Campbell, "Evaluation of a nanoscale zero-valent iron amendment as a potential tool to reduce mobility, toxicity, and bioaccumulation of arsenic and mercury from wetland sediments," \*Environmental Science and Pollution Research\*, vol. 27, pp. 18757-18772, 2020.
- [7] R. Jing, S. Fusi, and B. V. Kjellerup, "Remediation of polychlorinated biphenyls (PCBs) in contaminated soils and sediment: State of knowledge and perspectives," \*Frontiers in Environmental Science\*, vol. 6, p. 79, 2018.

- [8] T. Pak et al., "Pore-scale investigation of the use of reactive nanoparticles for in situ remediation of contaminated groundwater source," \*Proceedings of the National Academy of Sciences USA\*, vol. 117, pp. 13366-13373, 2020.
- [9] D. T. Pilipović et al., "Remediation of toxic metal contaminated sediment using three types of nZVI supported materials," \*Bulletin of Environmental Contamination and Toxicology\*, vol. 101, pp. 725-731, 2018.
- [10] Kamal, A., Ashmawy, M., Algazzar, A. M., & Elsheikh, A. H. Fabrication techniques of polymeric nanocomposites: a comprehensive review," Proceedings of the Institution of Mechanical Engineers, Part C: Journal of Mechanical Engineering Science 2022, vol. 236, no. 9, pp. 4843–4861, DOI:10.1177/09544062211055662.
- [11] T. Wang et al., "In-situ remediation of hexavalent chromium contaminated groundwater and saturated soil using stabilized iron sulfide nanoparticles," Journal of Environmental Management\*, vol. 231, pp. 679-686, 2019.
- [12] A. M. Alsaad et al., "Optical Properties of Transparent PMMA-PS/ZnO NPs Polymeric Nanocomposite Films: UV-Shielding Applications," Materials Research Express, vol. 6, p. 126446, 2020, doi: 10.1088/2053-1591/ab68a0.
- [13] I. Jum'h et al., "Optical and Structural Properties of (PANI-CSA-PMMA)/NiNPs Nanocomposites Thin Films for Organic Optical Filters," \*Journal of Applied Polymer Science, vol. 137, p. 48643, 2019, doi: 10.1002/app.48643.
- [14] H. Chamroukhi et al., "Optical and Structural Properties Enhancement of Hybrid Nanocomposites Thin Films Based on Polyaniline Doped with Zinc Oxide Embedded in Bimodal Mesoporous Silica (ZnO@SiOX) Nanoparticles," Optical Materials, vol. 84, pp. 703-713, 2018, doi: 10.1016/j.optmat.2018.07.041.
- [15] E. Sheha et al., "Dielectric and Optical Properties of p-Type (PVA/CuI) Nanocomposite Polymer Electrolyte for Photovoltaic Cells," Optik, vol. 123, pp. 1161-1166, 2012, doi: 10.1016/j.ijleo.2011.06.066.
- [16] S. Virtanen et al., "Modified Nano Fibrillated Cellulose-Polyvinyl Alcohol Films with Improved Mechanical Performance," \*RSC Advances\*, vol. 4, pp. 11343-11350, 2014, doi: 10.1039/c3ra46287k.
- [17] Y. H. Gad, H. E. Ali, and E. S. A. Hegazy, "Radiation-induced Improving Mechanical and Thermal Properties of Carboxymethyl Cellulose/Clay Composite for Application in Removal of Copper (II) Ions from Wastewater," \*Journal of Inorganic and Organometallic Polymers and Materials\*, vol. 31, pp. 2083-2094, 2021, doi: 10.1007/s10904-020-01850-w.
- [18] A. Pettignano, A. Charlot, and E. Fleury, "Solvent-Free Synthesis of Amidated Carboxymethyl Cellulose Derivatives: Effect on the Thermal Properties," \*Polymers\*, vol. 11, p. 1227, 2019, doi: 10.3390/polym11071227.

- [19] N. F. Mazuki et al., "Studies on Ionics Conduction Properties of Modification CMC-PVA Based Polymer Blend Electrolytes via Impedance Approach," \*Polymer Testing\*, vol. 81, p. 106234, 2020, doi: 10.1016/j.polymertesting.2019.106234.
- [20] K. Suppiah et al., "Properties and Characterization of Carboxymethyl Cellulose/Halloysite Nanotube bio-Nanocomposite Films: Effect of Sodium Dodecyl Sulfate," \*Polymer Bulletin\*, vol. 76, pp. 365-386, 2019, doi: 10.1007/s00289-018-2392-0.
- [21] M. C. Surette and J. A. Nason, "Effects of surface coating character and interactions with natural organic matter on the colloidal stability of gold nanoparticles," \*Environmental Science: Nano\*, vol. 3, pp. 1144-1152, 2016.
- [22] X. He et al., "Toxicity of engineered nanomaterials mediated by nano-bio-eco interactions," \*Journal of Environmental Science and Health, Part C\*, vol. 36, pp. 21-42, 2018.
- [23] A. S. Adeleye et al., "Engineered nanomaterials for water treatment and remediation: costs, benefits, and applicability," \*Chemical Engineering Journal\*, vol. 286, pp. 640-662, 2016, doi: 10.1016/j.cej.2015.10.105.
- [24] L. L. Tayo, "Stimuli-responsive nanocarriers for intracellular delivery," \*Biophysical Reviews\*, vol. 9, no. 6, pp. 931-940, 2017, doi: 10.1007/s12551-017-0341-z.
- [25] X. Hu et al., "Multifunctional gold nanoparticles: a novel nanomaterial for various medical applications and biological activities," Frontiers in Bioengineering and Biotechnology, vol. 8, p. 990, 2020, doi: 10.3389/fbioe.2020.00990.
- [26] D. G. Prajapati and B. Kandasubramanian, "Biodegradable Polymeric Solid Framework-Based Organic Phase-Change Materials for Thermal Energy Storage," Industrial & Engineering Chemistry Research, vol. 58, pp. 10652-10677, 2019, doi: 10.1021/acs.iecr.9b01693.
- [27] P. A. Hernley et al., "Engineering the Optical and Catalytic Properties of Co-Catalyst/Semiconductor Photocatalysts," \*ACS Photonics\*, vol. 4, pp. 979-985, 2017, doi: 10.1021/acsphotonics.7b00047.
- [28] S. A. Nouh et al., "Effect of Gamma Irradiation on the Structure, Optical and Thermal Properties of PC– PBT/NiO Polymer Nanocomposites Films," Journal of Inorganic and Organometallic Polymers and Materials\*, vol. 27, pp. 1851, 2017, doi: 10.1007/s10904-017-0650-5.
- [29] R. V. Navakoteswara et al., "Monodispersed Core/Shell Nanospheres of ZnS/NiO with Enhanced H2 Generation and Quantum Efficiency at Versatile Photocatalytic Conditions," \*Journal of Hazardous Materials\*, vol. 413, p. 125359, 2021, doi: 10.1016/j.jhazmat.2021.125359.

- [30] S. A. Nouh and K. Benthami, "Gamma Induced Changes in the Structure and Optical Properties of ZnS/PVA Nanocomposite," \*Journal of Vinyl and Additive Technology\*, vol. 25, pp. 271, 2019, doi: 10.1002/vnl.21689.
- [31] D. Bakeer et al., "Effect of Laser Radiation on the Linear and Nonlinear Optical Characteristics of Polyvinyl Alcohol/Carboxymethyl Cellulose/Nickel Oxide Nanocomposite Films," \*Journal of Macromolecular Science, Part B: Physics\*, vol. 62, pp. 718-737, 2023, doi: 10.1080/00222348.2023.2245301.
- [32] A. A. Alhazime et al., "PANI-Ag/PVA Nanocomposite: Gamma Induced Changes in the Thermal and Optical Characteristics," \*Journal of Vinyl and Additive Technology\*, vol. 27, pp. 47-53, 2021, doi: 10.1002/vnl.21782.
- [33] B. Karthikeyan et al., "Studies on NiO-PVA Composite Films for Opto-Electronics and Optical Limiters," \*IEEE Photonics Technology Letters\*, vol. 30, pp. 1539-1542, 2018, doi: 10.1109/LPT.2018.2859042.
- [34] S. A. Nouh et al., "Structural and Optical Characteristics of Laser Irradiated CdSe/PVA Nanocomposites," \*International Polymer Processing\*, vol. 34, pp. 255-261, 2019, doi: 10.3139/217.3729.
- [35] R. Singh, K. S. Samra, R. Kumar, and L. Singh, "Microstructural modifications in swift ion irradiated PET," Radiation Physics and Chemistry, vol. 77, pp. 575–580, 2008.
- [36] T. Steckenreiter, E. Balanzat, H. Fuess, and C. Trautmann, "Chemical modifications of PET induced by swift heavy ions," Nuclear Instruments and Methods in Physics Research B, vol. 131, pp. 159-166, 1997.
- [37] H. S. Virk and A. K. Srivastava, "Modification of optical, chemical and structural response of CR-39 polymer by 50 MeV lithium-ion irradiation," Radiation Measurements, vol. 34, pp. 65–67, 2001.
- [38] Y. H. Lee, C. A. Kim, W. H. Jang, H. J. Choi, and M. S. Jhon, "Synthesis and electrorheological characterizations of microencapsulated polyaniline particles with melamine-formaldehyde resins," Polymer, vol. 42, pp. 8277-8283, 2001.
- [39] A. Babazadeh Mirzaagha, "Direct One-pot Method for Synthesis of Polyaniline Doped with Dodecyl Benzene Sulphonic Acid in Aqueous Medium and Study of its Thermal Properties," Iranian Polymer Journal, vol. 16, pp. 389-396, 2007.
- [40] C. Peng, J. Jin, and G. Z. Chen, Electrochim. Acta 53, 525 (2007).
- [41] S. Jussila, M. Puustinen, T. Hassinen, J. Olkkonen, H. G. O. Sandberg, and K. Solehmainen, Org. Electron. 13, 1308 (2012).
- [42] P. J. Hung, K. H. Chang, Y.F. Lee, C.C. Hu, and K.M. Lin, Electro-chim. Acta 55, 6015 (2010).